Nanoindentation Study of Bulk Zirconium Hydrides at Elevated Temperatures[1]

M. Nedim Cinbiz[1], Mehdi Balooch[2], Xunxiang Hu[1], Aida Amroussia[1,3], and Kurt Terrani[1]

[1] Oak Ridge National Laboratory, Oak Ridge, TN 37831

[2] University of California, Berkeley, CA 94720

[3] Michigan State University, East Lansing, MI 48824

Abstract

The mechanical properties of zirconium hydrides were studied using nano-indentation technique between 25 and 400 °C. Temperature dependency of reduced elastic modulus and hardness of δ- and ε-zirconium hydrides were obtained by conducting nanoindentation experiments on bulk hydride samples with independently heating capability of indenter and heating stage. The reduced elastic modulus of δ-zirconium hydride (H/Zr ratio =1.61) decreased from ~113 GPa at room temperature to ~109 GPa at 400°C, while its hardness decreased significantly from 4.1 GPa to 2.41 GPa in the same temperature range. For ε-zirconium hydrides (H/Zr ratio=1.79), the reduced elastic modulus decreased from 61 GPa at room temperature to 54 GPa at 300 °C, while its hardness from 3.06 GPa to 2.19 GPa.

Keywords: Zirconium hydrides, bulk hydride, nanoindentation, temperature dependent elastic modulus, δ hydrides, reduced elastic modulus

1. Introduction

Zirconium hydrides may embrittle the zirconium-alloy nuclear fuel cladding during any stage of the nuclear fuel cycle [1,2], which would compromise the mechanical integrity of nuclear fuel rods at operation (in-pile) and storage/transportation (out-pile) conditions. During nuclear reactor operation, the zirconium-based alloy nuclear fuel cladding undergoes water-side corrosion reactions which cause cladding oxidation and hydrogen release [3]. Some portion of the released hydrogen is uptaken by the cladding. When the uptaken hydrogen reaches its solubility limit in zirconium at a specific temperature, it forms zirconium hydride precipitates, such as hydride rim (a dense hydride platelet region)[4], blister (bulk hydride)[5], circumferential and/or radial hydride platelets [6]. The presence of these features may worsen the mechanical behavior of the cladding by crack initiation and loss-of-ductility during in-pile and out-pile conditions.

During light-water reactor operating conditions, the continuously uptaken hydrogen starts to precipitate when hydrogen content reaches to solubility limit at elevated temperatures such as 300°C (i.e., the solubility limit of hydrogen is approximately 100 wt. ppm at 300°C [7]). Because hydride formation can start at higher temperature during reactor operation, the determination of temperature dependent mechanical properties of hydrides is essential.

There are three major zirconium hydride ZrH_r phases (where r is the stoichiometry coefficient): (i) FCT γ phase ($c/a>1$) with $r=1$ (ii) FCC δ phase with r in the range of 1.31 to 1.7, and (iii) FCT ε phase ($c/a<1$) with $1.7 < r < 2$ [8], where c and a refer to the dimensions of the crystal lattice. Amongst them, δ-hydride is the most observed and technologically important

phase for nuclear fuel cladding. Although other phases have also been observed at very high hydrogen contents in zirconium-alloy claddings [4].

Characteristics of δ-hydride precipitation and dissolution can be formulated by elastic-plastic accommodation energy evolution of a misfitting precipitate [9] during hydrogen-to-hydride (precipitation) or hydride-to-hydrogen (dissolution) phase transformations [10–16]. Because δ-hydride platelets have large anisotropic stress-free misfit strains associated by 17% volume difference between δ-hydride and α-zirconium crystals [17,18], the total strain energy of the hydride and matrix is to be reduced by elastic deformation of coherent hydride and matrix until reaching a critical size and then after elastic-plastic deformation of hydride and matrix [9] Solutions of these problems specify that the total (elastic and plastic parts) accommodation energy of the matrix-precipitate system depends on the mechanical properties of the matrix and the hydrides, especially hydride elastic modulus and yield stress during phase transformation [11,13].

The mechanical properties of δ-hydrides have been studied by several techniques such as internal friction measurements, tensile testing, ultrasonic pulse-echo, and hardness including micro- and nano- indentation [19–22]. Internal friction data highly depends on the dislocation density of the samples and the effects caused by dislocation density is to be analyzed to determine the hydride elastic properties [23]. Pulse-echo technique requires large samples for accurate measurements with many independent measurements, and also well-defined sample geometries to approximate the plane-wave solutions [24]. The resolution of micro-hardness is low to resolve the effects of the microstructural features, such as cracks and void-like defects as well [25]. Amongst these tecniques, nanoindentation enables reliable and reproducible measurements at locations where surface cracks and void-like defects are not present [25]. The

purpose of this study is to investigate the temperature dependency of hardness and reduced elastic modulus ($E^*=E/(1-\nu^2)$ of δ- and ε- hydrides phases, where E is the elastic modulus and ν is the Poisson's ratio), using nanoindentation measurements on bulk hydride samples. Bulk hydrides of varying stoichiometry were prepared by gaseous diffusion at elevated temperatures and tested for this study. The results from this investigation will support the formulation of computational studies of elastic-plastic accommodation energy evolution of a misfitting precipitate in a parent phase.

2. Method and Procedures

2.1.Materials and Methods

This study employs bulk specimens that contain more than 89 wt. % of δ- and/or ε-hydride and less than 11 wt. % of α-zirconium phases. Samples were prepared by gaseous diffusion of hydrogen into disc-shaped Zircaloy-4 samples with a diameter of 12.7 mm and nominal compositions of: Zr–1.27Sn–0.22Fe–0.11Cr– 0.118O–0.016C–0.01Si and [26]. Samples were placed on a quartz boat and into a stainless-steel vacuum chamber after removal of the native oxide layer by mechanical polishing. The chamber was initially evacuated down to 4 mTorr to produce an oxygen-free environment, followed by several purges using ultra-high purity argon (99.999%). Subsequently, hydrogen with a purity of 99.9995% was introduced into the sealed chamber up to the pre-calculated pressure at room temperature. The chamber was heated up to 400 °C at a rate of 10 °C/s and from 400 to 800 °C at a rate of 2.5 °C/min to avoid possible cracking.

Table 1 shows the hydrogen content of samples as determined by vacuum extraction method by Luvak Inc. (Boylston, MA). Using hydrogen contents and nominal composition of the alloy, stoichiometry coefficients were estimated as 1.61 for sample 1 and 1.79 for sample 2.

Table 1 Hot vacuum extraction results of samples and predicted stoichiometry ratios

Sample	Hydrogen Content [wt. ppm]	Accuracy ± [wt. ppm]	Weight [g]	r	r_{max}	r_{min}
1	17038	341	0.02543	1.61	1.64	1.58
2	16978	378	0.03745	1.79	1.83	1.75

X-ray diffraction patterns were acquired from the bulk hydride samples to identify the crystalline phases present. XRD powder samples of zirconium hydride were prepared on zero-background silicon single-crystal wafers. A small amount of Si SRM640d powder was added to the samples when collecting XRD patterns for sample displacement corrections. All XRD patterns were collected using a 0.30 kW (30 kV and 10 mA) D2 Phaser, Bruker Inc., XRD instrument equipped with Cu Kα radiation.

Fig. 1 shows powder XRD patterns of bulk samples used in the study. Bulk hydride sample with r=1.79 consisted only of ε-hydrides (see Fig. 1a); whereas, α-zirconium and δ-hydride peaks were indexed in the bulk hydride sample with nominal stoichiometry of 1.61.

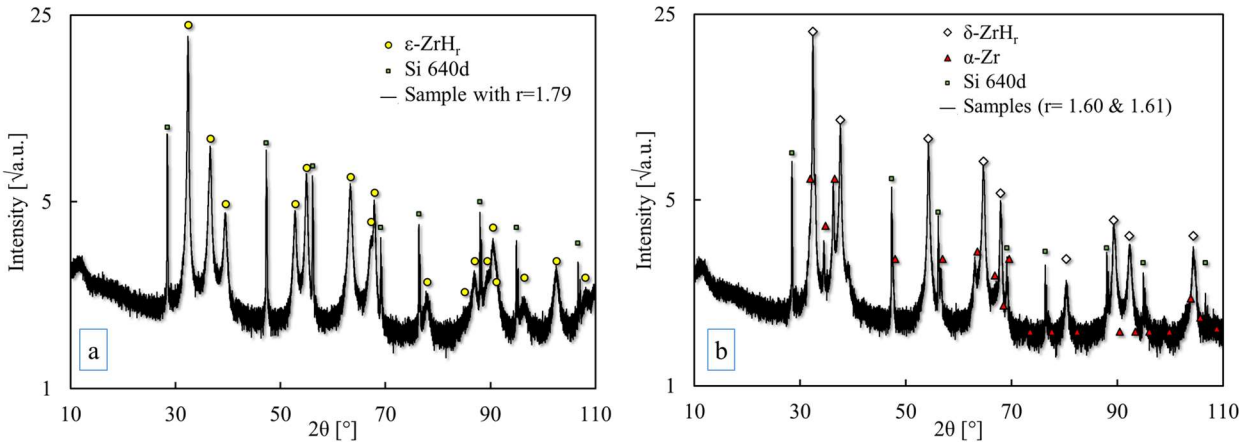

Fig. 1 X-ray diffraction patterns of bulk hydride samples employed in this study (a) sample with only ε-hydride (r=1.79) and (b) sample with a mixture of δ-hydride and α-zirconium (r=1.61).

To characterize the microstructure of bulk hydride samples, an electron back-scattering diffraction (EBSD) analysis (Fig. 2) was performed for δ-hydride bulk samples, while scanning electron microscopy (SEM) images were obtained for ε-hydride bulk sample[2] (Fig. 3). EBSD was performed using a JEOL JSM 6500F microscope with a field emission gun, equipped with an orientation imaging microscopy analysis system. The accelerating voltage was 20 kV; the working distance was 15 mm. The EBSD analysis indexed red areas in Fig. 1 as α-zirconium and the rest as δ-hydride. The average size of the equaxed δ hydride grains was 5 μm. SEM image of ε-hydrides (Fig. 3) revealed the existence of a band structure, consistent with previously published results [27]. It was also found that microcracks were present on the sample surface (white arrows in Fig. 3). One of two δ and ε hydride samples contained macroscopic surface cracks. Furthermore, ε-hydride sample contained microcracks with average length of 1.43μm (maximum and minimum lengths are 3.63 μm and 0.73 μm, respectively)(see Fig. 3), while no cracks were observed on the surface of the δ-hydride sample. Noting that, both δ and ε bulk

[2] For ε hydrides, roughness of the specimen surface prevented EBSD .

samples had polycrystalline microstructure and indentations were applied to several grains at the same time

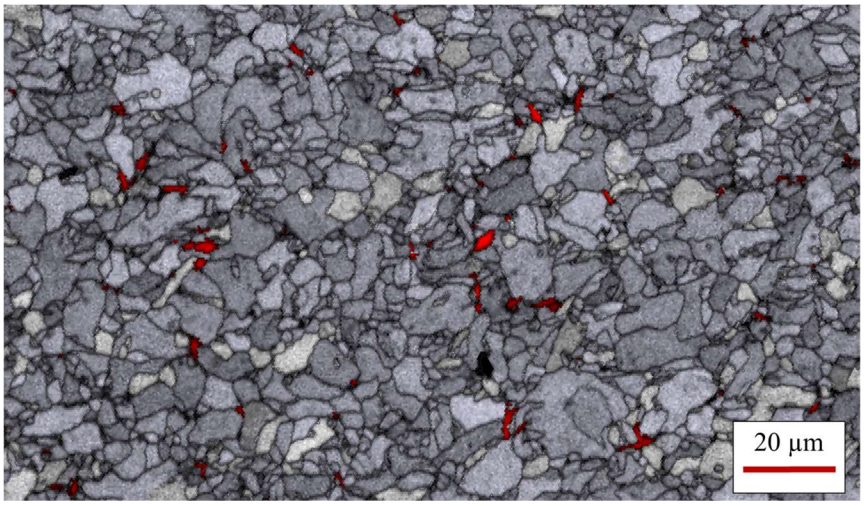

Fig. 2 EBSD map of representative microstructure of the bulk hydride samples with r=1.60 and 1.61 containing δ-hydrides and α-zirconium; the areas colored in red correspond to α-zirconium.

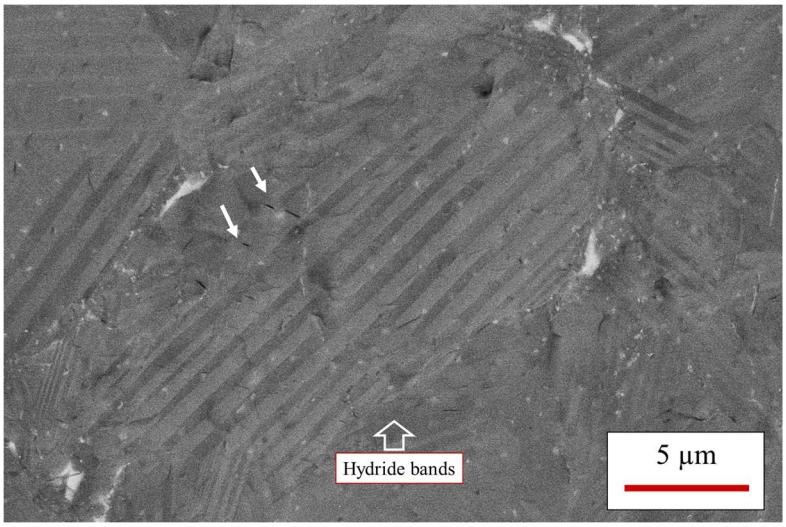

Fig. 3 SEM picture of sample (r=1.79) containing ε-hydrides (band structure). White arrows point to microcracks.

Fig. 4 depicts the indentation marks on the sample surfaces of δ hydride sample. Similar pattern was also applied to the bulk ε hydride sample as well. Indentation measurements were obtained at macroscopic crack-free regions of the ε hydrides. However, microscopic cracks, as shown in Fig. 3, may not be avoided for ε hydrides in the indent area because of the large indent mark size compared to microscopic crack sizes.

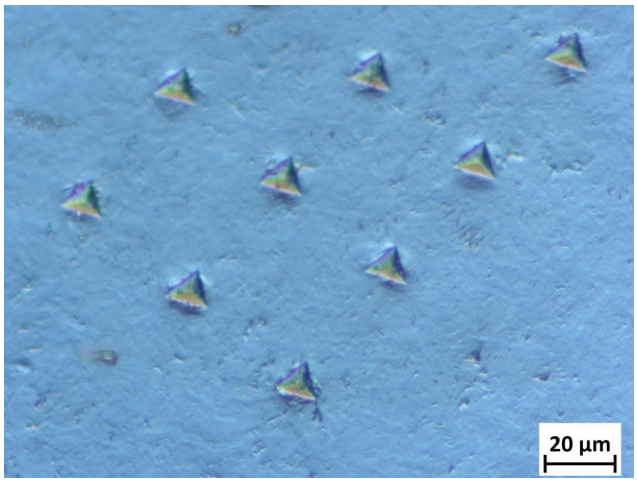

Fig. 4 (a) Optical image of indentation (8 by 8 matrix) on a representative sample surface that contains δ-hydrides and α-zirconium. Same indentation pattern was applied to the ε hydride sample.

Prior to the nanoindentation experiments, samples attached to the sample holder were ground with SiC papers of increasingly finer grit size, starting from 500 to 1200 grit size and then were polished with 0.01 micron alumina paste using VibroMet 2 Vibratory Polisher (BUEHLER) for 12 hours for high quality polished surfaces.

2.2.Room and High Temperature Nanoindentation Experiments

Nanoindentation experiments at ambient and elevated temperatures were performed using a Micro Materials Ltd. nanoindenter for bulk hydride specimens with r values of 1.61 and 1.79. the indenter had a diamond Berkovich tip with tip radius of 12 nm. The instrument was equipped with a high temperature stage which enabled to control active heating of the indenter and sample independently when conducting tests at elevated temperatures. This capability ensured thermal equilibrium, avoided heat flow during experiments, and reduced thermal drift [28]. In order to prevent sample oxidation, the nano-indenter operated in a argon gas environment. The chamber was purged with a flow rate of 3 L/min for 24 hours while specimens were present before heating. Prior to high-temperature tests, nanoindentation was performed at ambient temperature. Also indentation data were collected as a function of the penetration depth of the indenter at ambient temperature. Each sample and the indenter were independently heated up to 100, 200, 300, and 400 °C with a heating rate of 3 °C/min for indentation measurements, respectively. At each measurement temperature, samples were kept in the indenter approximately for two hours to achieve thermal equilibration before measurements.

In the study, single load-displacement tests were performed to determine the elastic moduli of the bulk hydride samples. The elastic moduli were calculated by applying the Olivier-Pharr formula Eq. (1),

$$E^* = \frac{\sqrt{\pi}}{2\beta}\frac{S}{\sqrt{A}}, \quad (1)$$

where E^* is the effective elastic modulus, β is a dimensionless parameter that accounts for the deviations in stiffness, and A is the contact area,

and Eq. (2),

$$\frac{1}{E^*} = \frac{1-\nu_s^2}{E_s} + \frac{1-\nu_i^2}{E_i}, \quad (2)$$

where E is the elastic modulus, ν is Poisson's ratio, s is the sample, and i is the indenter.

The dimensionless parameter β, which accounts for deviations in stiffness, is taken as 1.034[3]; A is the contact area determined by areal function determination on well know sample such as Silica to determine the geometry of the indenter;

The contact depth, h_p, is determined by Eq. (3),

$$h_p = h_{max} - \varepsilon P_{max}/S, \quad (3)$$

where ε is assumed to be 0.73 for a Berkovich indenter (approximately 150 nm radius of curvature) and S is the contact stiffness, which is calculated from the initial slope of the unloading load-displacement curve (Eq. 4).

$$S = \left(\frac{dP}{dh_p}\right)_{h_{p,max}} \quad (4)$$

In this manuscript, we report nanoindentation measurement data in terms of the reduced elastic modulus of δ-hydrides:

$$E^* = E_{hyd}/(1-\nu_{hyd}^2) \quad (5)$$

3. Results and Discussion

Nanoindentation measurement were performed on bulk hydride samples at ambient and elevated temperatures to investigate the temperature dependency of the reduced elastic modulus and hardness of δ-hydrides. Fig. 5 shows the dependence of the reduced elastic modulus and hardness of hydrides on the penetration depth at room temperature. As shown in Fig. 5a, for both

[3] Uncertainty related to the value of β is much smaller than uncertainty associated with Poisson's ratio of hydrides

δ and ε hydrides the magnitude of the reduced modulus decreases as the penetration depth increases up to 800 nm due to indentation size effect (ISE). For penetration depths greater than 800 nm, the reduced modulus is independent of penetration depth. Similar behavior was also observed for hardness at penetration distances of 400 nm as shown in Fig. 5b.

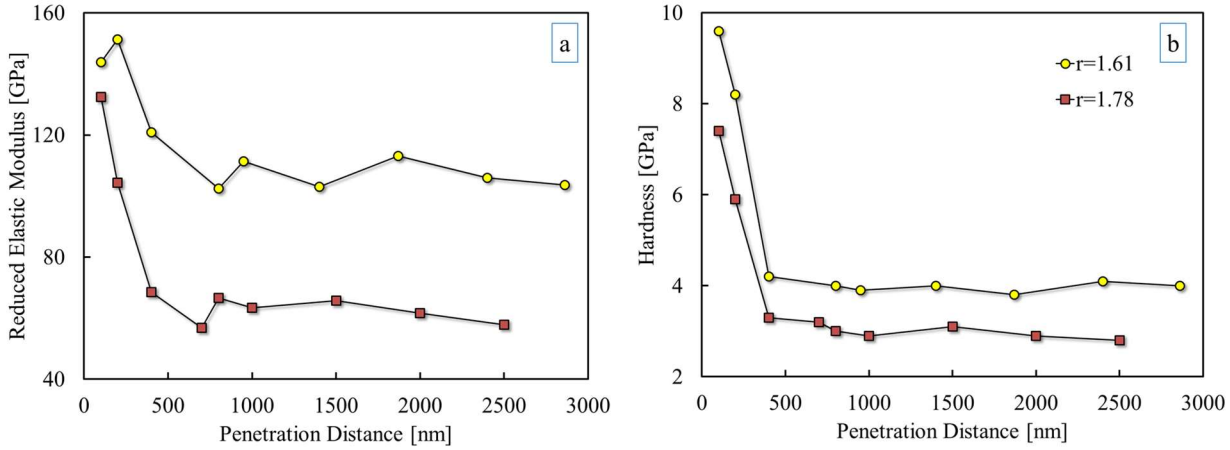

Fig. 5 Dependence of (a) reduced elastic modulus and (b) hardness on penetration depth at ambient conditions.

The room-temperature values for elastic modulus and hardness of δ- and ε-hydrides are shown in Table 2. The reduced elastic modulus and hardness of δ-hydrides were determined to be higher than those of ε-hydrides. Table 2 also depicts the change in elastic modulus for distinct ν values. As ν increases from 0.2 to 0.37, the elastic modulus decreases for δ- and ε-hydrides.

Table 2 Room temperature results of and hardness*

Hydride	r	$E/(1-\nu^2)$ [GPa]	H [GPa]	E (ν=0.2)	E (ν≈0.32) [20]	E (ν=0.37) [19]
δ	1.61	112.92 ±2.7	4.1 ±0.2	108.4	101.36	97.46
ε	1.79	61.42 ±2.79	3.06 ±0.18	58.97	55.13	53.01

* Yamanaka et al. reported ν values for δ-hydrides in the range of 0.317- to 0.322 for bulk δ-hydride samples. The data were obtained by employing an ultrasound pulse-echo technique [20]. The ultrasonic data are decoupled to determine appropriate ν for δ-hydrides to eliminate the uncertainty associated with a mixed microstructure [20] of α-zirconium and δ-hydrides, such as shown in Fig. 1. To our knowledge, the the findings of Yamanaka et al. are the only existing experimental data on hydride ν values. Rico et al. utilized Poisson's ratio of ZIRLO™ (0.37) in their study of δ-hydrides [19].

Fig. 6 shows the temperature-dependent reduced elastic modulus of bulk hydride samples. The reduced modulus of δ-hydride (Fig. 6a) was found to be greater than that of ε-hydride (Fig. 6b), which is consistent with reported values [19,22]. The reduced elastic modulus of δ-hydrides (r=1.61) decreased from ~113 GPa to ~109 GPa while temperature increased from room temperature to 400 °C, a 3.5% drop. For ε-hydrides, the elastic modulus decreased from 61 GPa to 54 GPa (a change of 11.4%) as temperature increased from room temperature to 300°C (see Fig. 6b).

The hardness of δ-hydrides, shown in Fig. 7, decreased substantially, from ~4 GPa to ~2.1 GPa (a 47.5% change), while temperature increased from room temperature to 400°C. For ε-hydrides, a similar trend was observed for hardness, which decreased from 3.06 GPa to 2.19 GPa as temperature increased from room temperature to 300°C. The change in the hardness was calculated as 28% (the change in δ-hydride hardness for same temperature range of ε-hydrides was calculated as 31.7%, which was similar).

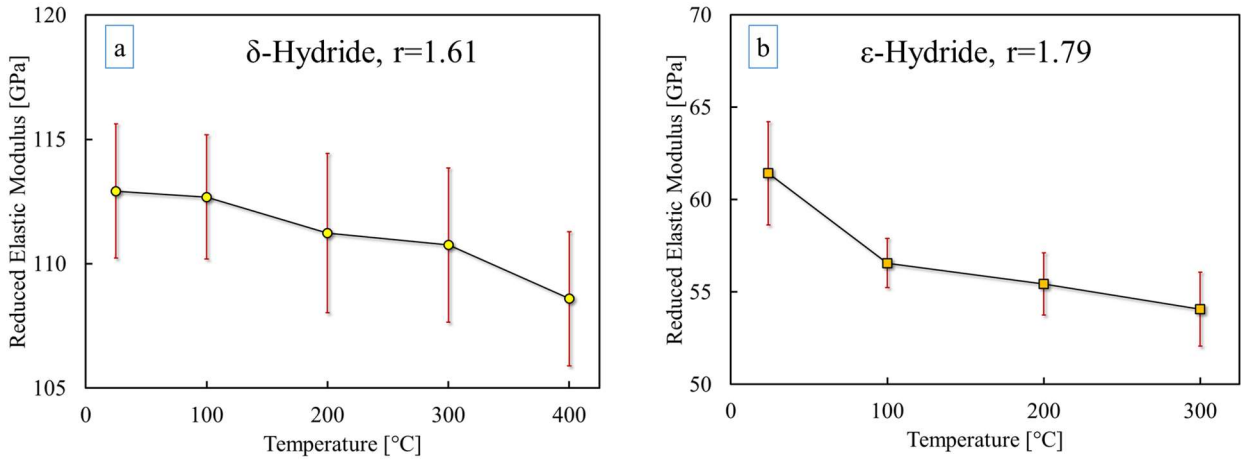

Fig. 6 Temperature dependent reduced elastic modulus of (a) δ and (b) ε hydrides. Data points correspond to average values from 64 measurements. Error bars correspond to one standard deviation about the mean values.

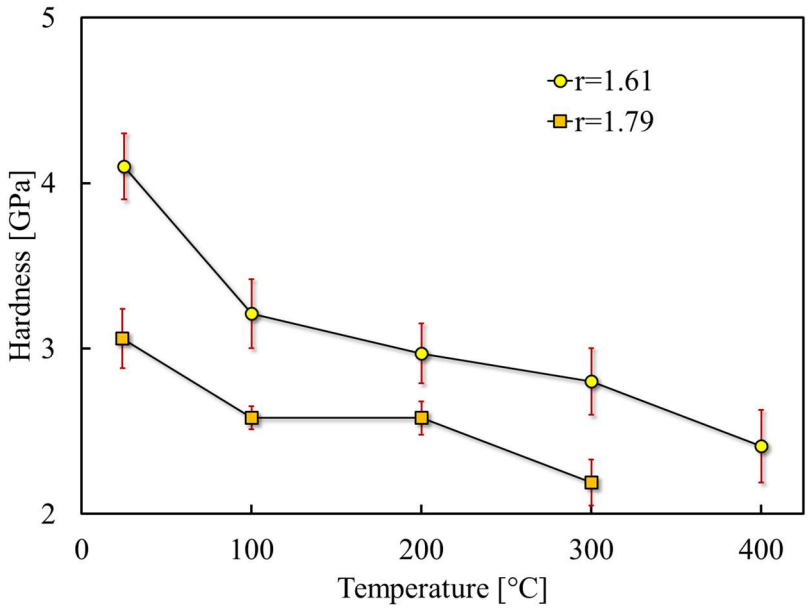

Fig. 7 Temperature dependent hardness of δ (r=1.61) and ε (r=1.79) hydrides. Data points correspond to average values from 64 measurements. Error bars correspond to one standard deviation about the mean values.

Because of adverse effects of oxidation on the nano-indentation measurements at elevated temperatures, oxygen profile was determined as a function of depth by x-ray photoelectron spectroscopy (XPS). Fig. 8a shows concentration depth profiles, which revealed a maximum in oxygen concentration over a depth of approximately 5 nm. Then the concentration of oxygen was found to decrease until reaching a constant concentration down to 24 nm, which was the maximum sputtering depth in these measurements. Similar results were found for ε-hydrides (see Fig. 8b), for which oxgen counts immediately started to decrease at 6 nm. Considering that the depth of penetration in these indentation measurements was greater than 500 nm, these results suggest that the oxide thickness had a negligible effect on the indentation measurements for both samples.

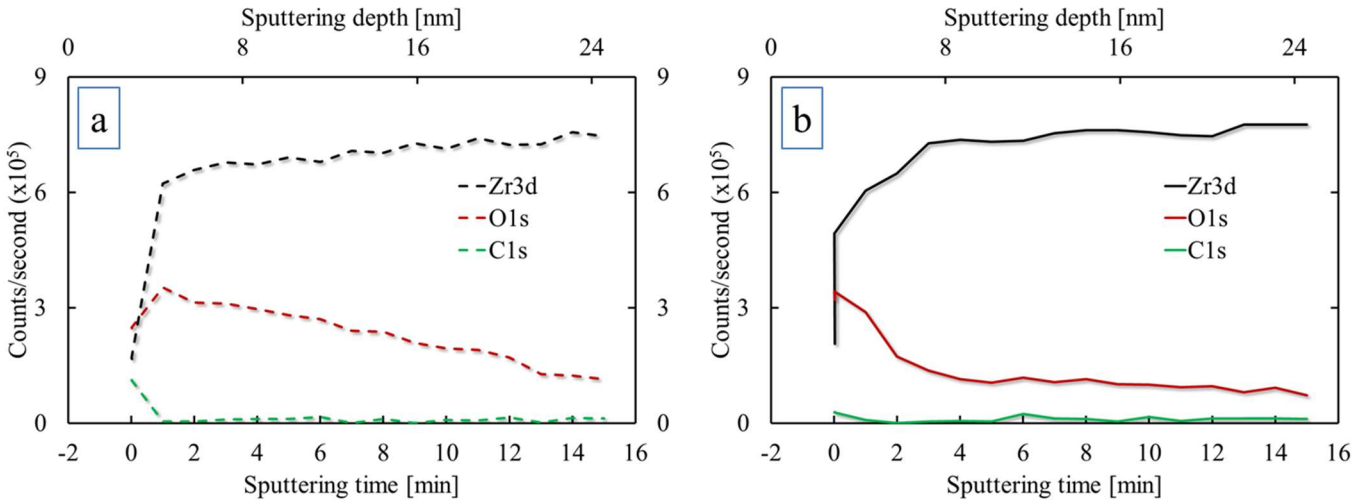

Fig. 8 XPS profile of (a) δ and (b) ε hydride samples after high-temperature nano-indentation measurements as a function of sputtering time and depth.

4. Discussion on δ-Hydride Mechanical Behavior

In Fig. 9 and *Fig. 10*, the elastic modulus and hardness results obtained for δ-hydrides in this study are compared with published results of tests carried out at room temperature. An overall tendency is the reduction of elastic modulus and hardness with increasing stoichiometry. The elastic modului of hydrides from nanoindentation results and direct reduced elastic modulus data were recalculated using a value of 0.37 for Poisson's ratio of hydrides [19]. The value for Poisson's ratio was chosen so that a direct comparison of our results could be made with the hydride blister data from ref [19].

Yamanaka et al. [20] and Terrani et al. [29] have determined the elastic modulus of δ-hydrides in the range of 120-140 GPa using ultrasonic pulse-echo and nanoindentation of mixed phase hydrides, respectiveley. Other nanoindentation studies by Rico et al. [19] and Menibus et al. [5] reported that the elastic modulus of δ-hydride is in the range of 90-110 GPa. Results of this study are similar to those reported from previous nanoindentation studies. Internal friction of "as-hydrided" samples [21] and confined uniaxial experiments of hydrided samples determined similar elastic modulus values as well, as shown in Fig. 9. Meanwhile, microhardness measurements predicted lower values that are close to the matrix elastic modulus [25]; likely due to the indenter resolution of micro hardness. Hence, the room temperature elastic modulus results of δ-hydrides in this study are consistent with results reported in literature, except from ref. [20,29].

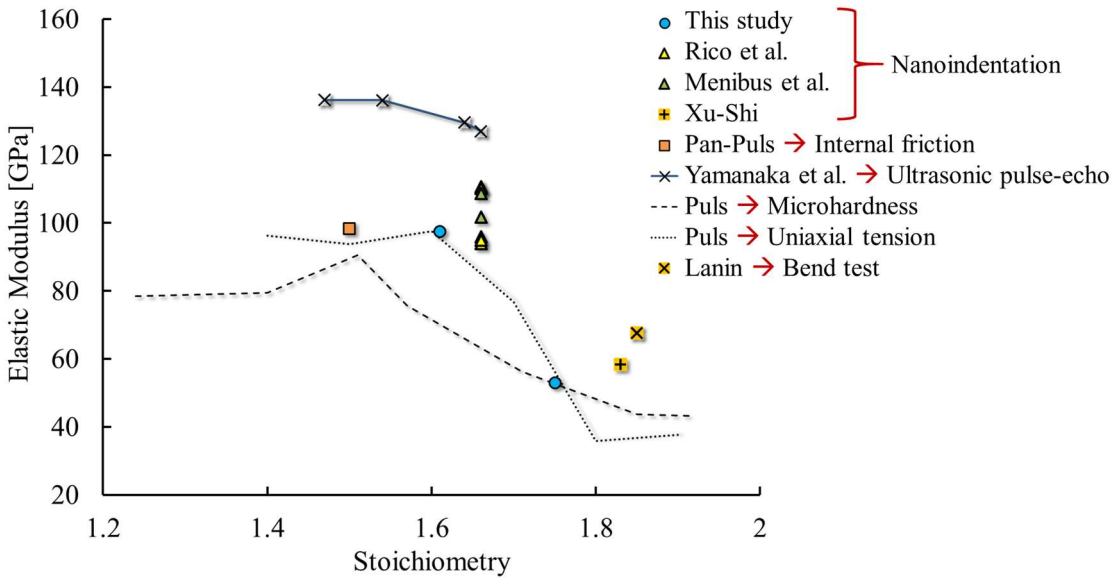

Fig. 9 Elastic modulus data of this study and reported in literature[4]. All reduced elastic modulus data of Rico [19], Puls et al. [30], Xu and Shi [22], Menibus et al. [5], and this study were re-calculated using Poisson's ratio ν=0.37 to compare results. Values of Yamanaka et al. [20], Pan and Puls [21], Puls, and Lanin [31] are directly determined by their measurement techniques.

Fig. 10 compares the room temperature hardness values obtained in this study with those reported in the literature, in particular results obtained with Berkovich indenter to eliminate variations that may result from the indenter shape. The results in Fig. 9 for hardness as a function of stoichiometry in the range between 1.5 and 1.86 are consistent with those reported for similar bulk hydride samples[22,27,32]; Oono et al., reported hardness value of ~1.5 GPa at a stoichiometry ratio of 1.97, which are significantly lower than those reported by others. These low values of hardness could be related to pre-existing cracks, as shown in Fig. 3, and/or crack nucleation around the indent, as determined by Oono et al. [33]. During indentation

[4] No computational studies were included in the graph. In thisd study, hydride blister's stoichiometry coefficient was accepted as 1.63 for studies of Rico et al. and Menibus et al.

measurements may abruptly increase the compliance of the materials and so elastic modulus and hardness of ε-hydride decreases as well. For hydride blister results, hardness of δ-hydrides are in the range of 2 GPa [19] and 6 GPa [5].

Reduction in the hardness with increasing temperature (total change is 47.5%), as shown in Fig. 7, is expected to be related to a sharp decrease in yield strength of hydrides in the temperature range of 25°C to 400°C. If we assume hardness is directly proportional to yield stress, then the room temperature yield stress of δ-hydrides decreases to approximately half of its value at 400°C. For instance, Rico et al. have determined the yield stress of δ-hydrides in the range of 600-700 MPa at room temperature by conducting nanoindentation measurements with spherical indent combined with a Hertz equation solution [34]. Based on the calculated results of yield stress reported by Rico et al. [34], the yield stress will decreases down to 300-350 MPa range at 400 °C. This value is still higher than that of most Zr-based cladding materials (strong function of alloy type and manufacturing process) at the same temperature, but substantially lower than the compressive stresses acting on δ-hydride precipitate during precipitation as determined by both calculation [11,16] and in situ x-ray diffraction experiments [35–37].

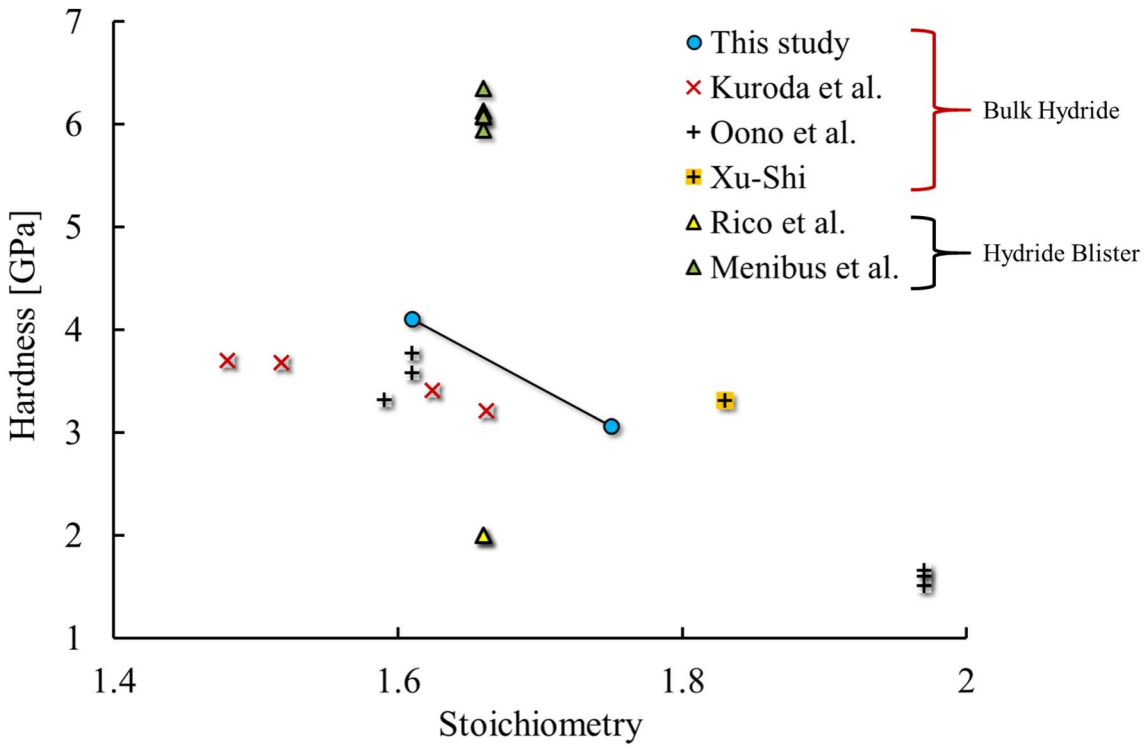

Fig. 10 Hardness values obtained by nanoindentation from this study and reported in the literature as a function of stoichiometry.

High temperature nanoindentation measurements revealed a weak temperature dependency of the elastic modulus. Fig. 11 compares data obtained from this study with measurements obtained by internal friction [21] and microhardness [30]. A lower elastic modulus has been determined for δ-hydrides by microhardness than by internal friction or nanoindentation. Due to the indenter resolution of the microhardness test, results are expected to be close to the elastic modulus of the α-zirconium matrix. Furthermore, the effect of surface features, such as voids, are likely to contribute to the results.

On the other hand, internal friction results of "as-hydrided" samples [21] are similar to temperature dependent nanoindentation measurements in this study. It should be remarked that

Pan and Puls have conducted internal friction experiments on "as-hydrided" and quenched samples [21]; The quenched samples have showed lower elastic modulus than the "as-hydrided" samples. It is likely because internal friction and dynamic modulus are susceptible to (i) nonlinear effect, (ii) the Köster effect, and (iii) viscosity effect that are addressed by dislocation theory, as addressed by Nowick [23]. In addition these effects are all functions of frequency, strain amplitude, temperature, recovery, and prior deformation of the specimen, which cause oscillatory response in dynamic modulus and distinct results of dynamic modulus depending on the dislocation microstructure [23]. A detailed discussion of these effects is beyond the scope of this study; but dynamic modulus is generally lower than the actual elastic modulus and can show oscillatory response [23]. By removing such effects as addressed by Nowick from the internal friction data analysis of the quenched samples, then it is expected that the oscillatory response of dynamic Young's modulus will be avoided. Thus, we only highlight internal friction results of the "as-hydrided" sample results to make a comparison.

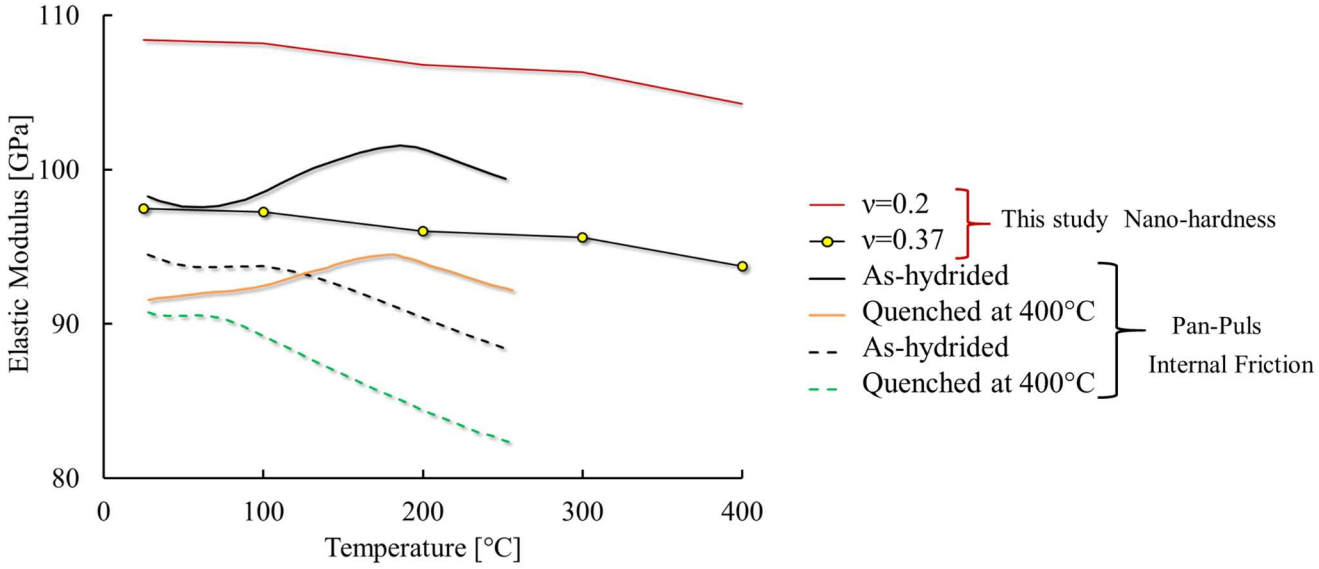

Fig. 11 Temperature dependent elastic modulus in this study and from the literature

5. Conclusions

In order to investigate the effect of temperature on the mechanical properties of hydrides, nanoindentation measurements were applied to δ and ε hydride bulk samples with independently heating capability of indenter and the sample stage. Results showed consistency with the existing literature values. The reduced elastic modulus showed a small decrease as a function of temperature up to 400°C; a 3.5% drop for δ-hydrides and 11.4% drop for ε-hydrides. Hardness of δ-hydride significantly decreased from 4.1 GPa to 2.41 GPa when temperature increased from room temperature to 400 °C. Similarly, hardness of ε-hydride decreased from 3.06 GPa to 2.19 GPa with temperature increase from room temperature to 300°C.

Reduction in the hardness with increasing temperature is anticipated to be associated with a sharp decrease in yield strength of hydrides in the temperature range of 25°C to 400°C. It is therefore concluded that to fully inform thermo-mechanical models describing Zr-based cladding behavior under in-pile and storage conditions, accurate yield strength data as a function of temperature for δ-hydrides is necessary for light-water reactor applications.

Acknowledgements

This material is based upon work supported by the U.S. Department of Energy, Office of Nuclear Energy, Advanced Fuels Campaign. Authors are thankful to Edgar Lara-Curzio at Oak Ridge National Laboratory for his valuable discussions.

References

[1] M. Billone, T. Burtseva, R. Einziger, Ductile-to-brittle transition temperature for high-burnup cladding alloys exposed to simulated drying-storage conditions, J. Nucl. Mater. 433 (2013) 431–448. doi:10.1016/j.jnucmat.2012.10.002.

[2] F. Nagase, T. Fuketa, Investigation of hydride rim effect on failure of Zircaloy-4 cladding with tube burst test, J. Nucl. Sci. Technol. 42 (2005) 58–65. doi:10.1080/18811248.2005.9726364.

[3] A.T. Motta, A. Couet, R.J. Comstock, Corrosion of zirconium alloys used for nuclear fuel cladding, Annu. Rev. Mater. Res. 45 (2015) 311–343. doi:10.1146/annurev-matsci-070214-020951.

[4] R.S. Daum, Y.S. Chu, A.T. Motta, Identification and quantification of hydride phases in Zircaloy-4 cladding using Synchrotron radiation diffraction, J. Nucl. Mater. 392 (2009) 453–463.

[5] A. Hellouin De Menibus, Q. Auzoux, O. Dieye, P. Berger, S. Bosonnet, E. Foy, V. Macdonald, J. Besson, J. Crépin, Formation and characterization of hydride blisters in Zircaloy-4 cladding tubes, J. Nucl. Mater. 449 (2014) 132–147. doi:10.1016/j.jnucmat.2014.03.006.

[6] C.E. Ells, Hydride precipitates in zirconium alloys (A review), J. Nucl. Mater. 28 (1968) 129–151. doi:10.1016/0022-3115(68)90021-4.

[7] A. McMinn, E.C. Darby, J.S. Schofield, The terminal solid solubility of hydrogen in zirconium alloys, in: G.P. Sabol, J. Moan (Eds.), Zircon. Nucl. Ind. Twelfth Int. Symp. ASTM STP 1354, American Society for Testing and Materials, Toronto, CA, 2000: pp. 173–195.

[8] E. Zuzek, J.P. Abriata, A. San-Martin, F.D. Manchester, The H-Zr (hydrogen-zirconium) system, Bull. Alloy Phase Diagrams. 11 (1990) 385–395. doi:10.1007/BF02843318.

[9] J.K. Lee, Y.Y. Earmme, H.I. Aaronson, K.C. Russell, Plastic relaxation of the transformation strain energy of a misfitting spherical precipitate: Ideal plastic behavior, Metall. Trans. A. 11 (1980) 1837–1847. doi:10.1007/BF02655099.

[10] M.P. Puls, Hydrogen induced delayed cracking: 2. effect of stress on nucleation, growth, and coarsening of zirconium hydride precipitates, AECL-8381. (1984) 30.

[11] B.W. Leitch, M.P. Puls, Finite element calculations of the accommodation energy of a misfitting precipitate in an elastic-plastic matrix, Metall. Trans. A (Physical Metall. Mater. Sci. 23A (1992) 797–806. doi:10.1007/BF02675557.

[12] M.P.P. Puls, The effects of misfit and external stresses on terminal solid solubility in hydride-forming metals, Acta Metall. 29 (1981) 1961–1968. doi:10.1016/0001-6160(81)90033-X.

[13] B.W. Leitch, S.-Q. Shi, Accommodation energy of formation and dissolution for a misfitting precipitate in an elastic - plastic matrix, Model. Simul. Mater. Sci. Eng. 4 (1996) 281–292. doi:10.1088/0965-0393/4/3/003.

[14] W. Qin, N.A.P. Kiran Kumar, J.A. Szpunar, J. Kozinski, Intergranular δ-hydride nucleation and orientation in zirconium alloys, Acta Mater. 59 (2011) 7010–7021. doi:10.1016/j.actamat.2011.07.054.

[15] W. Qin, J.A.A. Szpunar, J. Kozinski, Hydride-induced degradation of hoop ductility in textured zirconium-alloy tubes: A theoretical analysis, Acta Mater. 60 (2012) 4845–4855. doi:10.1016/j.actamat.2012.06.003.

[16] R.N. Singh, H.K. Khandelwal, A.K. Bind, S. Sunil, P. Ståhle, Influence of stress field of

expanding and contracting plate shaped precipitate on hydride embrittlement of Zr-alloys, Mater. Sci. Eng. A. 579 (2013) 157–163. doi:10.1016/j.msea.2013.04.117.

[17] G.J.C. Carpenter, The dilatational misfit of zirconium hydrides precipitated in zirconium, J. Nucl. Mater. 48 (1973) 264–266. doi:10.1016/0022-3115(73)90022-6.

[18] R.N. Singh, P. Ståhle, A.R. Massih, A.A. Shmakov, Temperature dependence of misfit strains of δ-hydrides of zirconium, J. Alloys Compd. 436 (2007) 150–154. doi:http://dx.doi.org/10.1016/j.jallcom.2006.07.049.

[19] A. Rico, M.A. Martin-Rengel, J. Ruiz-Hervias, J. Rodriguez, F.J. Gomez-Sanchez, Nanoindentation measurements of the mechanical properties of zirconium matrix and hydrides in unirradiated pre-hydrided nuclear fuel cladding, J. Nucl. Mater. 452 (2014) 69–76. doi:10.1016/j.jnucmat.2014.04.045.

[20] S. Yamanaka, K. Yoshioka, M. Uno, M. Katsura, H. Anada, T. Matsuda, S. Kobayashi, Thermal and mechanical properties of zirconium hydride, J. Alloys Compd. 293–295 (1999) 23–29. doi:10.1016/S0925-8388(99)00389-8.

[21] Z.L. Pan, M.P. Puls, Internal friction peaks associated with the behaviour of hydrogen in Zr and Zr–2.5Nb, Mater. Sci. Eng. A. 442 (2006) 109–113. doi:10.1016/j.msea.2006.02.211.

[22] J. Xu, S.Q. Shi, Investigation of mechanical properties of epsilon-zirconium hydride using micro- and nano-indentation techniques, J. Nucl. Mater. 327 (2004) 165–170.

[23] A.S. Nowick, Internal friction and dynamic modulus of cold-worked metals, J. Appl. Phys. 25 (1954) 1129–1134. doi:10.1063/1.1721827.

[24] R.G. Leisure, F.A. Willis, Resonant ultrasound spectroscopy, J. Phys. Condens. Matter. 9 (1997) 6001. http://stacks.iop.org/0953-8984/9/i=28/a=002.

[25] M.P. Puls, The Effect of Hydrogen and Hydrides on the Integrity of Zirconium Alloy Components, Electronic, Springer London, London, 2012. doi:10.1007/978-1-4471-4195-2.

[26] X. Hu, K.A. Terrani, B.D. Wirth, Hydrogen desorption kinetics from zirconium hydride and zirconium metal in vacuum, J. Nucl. Mater. 448 (2014) 87–95. doi:10.1016/j.jnucmat.2014.01.028.

[27] N. Oono, R. Kasada, T. Higuchi, K. Sakamoto, M. Nakatsuka, A. Hasegawa, S. Kondo, N.Y. Iwata, H. Matsui, A. Kimura, Comparison of irradiation hardening and microstructure evolution in ion-irradiated delta and epsilon hydrides, J. Nucl. Mater. 442 (2013) S826–S829. doi:10.1016/j.jnucmat.2013.03.013.

[28] N.M. Everitt, M.I. Davies, J.F. Smith, High temperature nanoindentation – the importance of isothermal contact, Philos. Mag. 91 (2011) 1221–1244. doi:10.1080/14786435.2010.496745.

[29] K.A. Terrani, G.W. Chinthaka Silva, C.B. Yeamans, M. Balooch, D.R. Olander, Fabrication and characterization of uranium–thorium–zirconium hydrides, J. Nucl. Mater. 392 (2009) 151–157. doi:10.1016/j.jnucmat.2009.03.031.

[30] M.P.P. Puls, S.-Q.Q. Shi, J. Rabier, Experimental studies of mechanical properties of solid zirconium hydrides, J. Nucl. Mater. 336 (2005) 73–80. doi:10.1016/j.jnucmat.2004.08.016.

[31] A.G. Lanin, I.M. Zalivin, V.N. Turchin, E.B. Boiko, Mechanical properties of zirconium, titanium, and yttrium hydride alloys, Strength Mater. 16 (1984) 869–876. doi:10.1007/BF01529980.

[32] M. Kuroda, D. Setoyama, M. Uno, S. Yamanaka, Nanoindentation studies of zirconium hydride, J. Alloys Compd. 368 (2004) 211–214. doi:10.1016/j.jallcom.2003.08.094.

[33] N. Oono, R. Kasada, T. Higuchi, K. Sakamoto, M. Nakatsuka, A. Hasegawa, S. Kondo, H. Matsui, A. Kimura, Irradiation hardening and microstructure evolution of ion-irradiated Zr-hydride, J. Nucl. Mater. 419 (2011) 366–370. doi:10.1016/j.jnucmat.2011.06.041.

[34] M.A. Martin Rengel, F.J. Gomez, A. Rico, J. Ruiz-Hervias, J. Rodriguez, Obtention of the constitutive equation of hydride blisters in fuel cladding from nanoindentation tests, J. Nucl. Mater. (2017). doi:10.1016/j.jnucmat.2017.02.001.

[35] M.S. Blackmur, M. Preuss, J.D. Robson, O. Zanellato, R.J. Cernik, F. Ribeiro, J. Andrieux, Strain evolution during hydride precipitation in Zircaloy-4 observed with synchrotron X-ray diffraction, J. Nucl. Mater. 474 (2016) 45–61. doi:10.1016/j.jnucmat.2016.01.039.

[36] M.N. Cinbiz, D.A. Koss, A.T. Motta, J.-S. Park, J.D. Almer, In situ synchrotron X-ray diffraction study of hydrides in Zircaloy-4 during thermomechanical cycling, J. Nucl. Mater. (2017). doi:10.1016/j.jnucmat.2017.02.027.

[37] K.B. Colas, A.T. Motta, M.R. Daymond, J.D. Almer, Effect of thermo-mechanical cycling on zirconium hydride reorientation studied in situ with synchrotron X-ray diffraction, J. Nucl. Mater. 440 (2013) 586–595. doi:http://dx.doi.org/10.1016/j.jnucmat.2013.04.047.

1